MOLECULAR AND CELLULAR BIOLOGY, Dec. 2009, p. 6245–6256 Vol. 29, No. 23
0270-7306/09/$12.00 doi:10.1128/MCB.00679-09

Loss of YY1 Impacts the Heterochromatic State and Meiotic Double-Strand Breaks during Mouse Spermatogenesis▽

Su Wu,[1]* Yueh-Chiang Hu,[2,3] Huifei Liu,[1] and Yang Shi[1]*

Department of Pathology, Harvard Medical School, Boston, Massachusetts 02115[1]; Whitehead Institute and Department of Biology, Massachusetts Institute of Technology, Cambridge, Massachusetts 02142[2]; and Department of Dentistry, School of Dentistry, National Yang-Ming University, Taipei, Taiwan[3]

Received 26 May 2009/Returned for modification 18 June 2009/Accepted 7 September 2009

The progression of spermatogenesis involves global changes in chromatin structure and conformation. However, our understanding of the regulation of chromatin changes in germ cells remains limited. Here we describe both in vivo RNA interference and genetic mouse knockout studies that identify a critical role for Yin Yang 1 (YY1) in mammalian spermatogenesis. In the YY1-deficient spermatocytes, we find a significant decrease in the global level of the heterochromatin markers (H3K9me3 and HP1-gamma) and a concomitant increase in the double-strand break (DSB) signals on chromosomes (gamma-H2AX, terminal deoxynucleotidyltransferase-mediated dUTP-biotin nick end labeling, and Rad51) at the leptotene/zygotene stages of spermatocytes. These findings support a link between chromatin modifications and meiotic DSB formation, as has been seen in other model organisms. We propose that a depletion of YY1 may alter the structural integrity of heterochromatin, rendering it more accessible to the DSB machinery. In addition, YY1-deficient spermatocytes show univalent formation, increased aneuploidy, and pachytene cell death, which are likely due to defects in DNA repair. Taken together, this study identifies an important role for YY1 in mouse meiosis and provides new insight into mechanisms that regulate mammalian spermatogenesis.

Meiosis is a specialized cell division in which two rounds of nuclear divisions succeed a single round of DNA duplication: the first division segregates homologous chromosomes, and the second division segregates sister chromatids, producing four haploid gametes (45). Before these divisions, homologous chromosomes are paired and held together by the synaptonemal complex (SC), and the exchange of genetic information occurs through meiotic recombination. Meiotic recombination begins with the programmed double-strand breaks (DSBs) (9, 60), followed by a specialized DSB repair mechanism using the homologous chromosomes as templates, and ultimately generates the crossovers between homologs for proper segregation. Work with a variety of model organisms has defined the importance of the core meiotic recombination components, the lack of which commonly lead to aneuploidy and cell death (25, 30).

YY1 is a ubiquitously expressed and multifunctional zinc-finger transcription factor and also a member of the evolutionarily conserved Polycomb group (PcG) protein family that plays critical roles in the maintenance of cell identity during development and differentiation through gene silencing (43). In vivo studies show that mammalian development and homeostasis are highly dependent on the dosage of the *YY1* gene (1), and constitutive knockout of the *YY1* gene in mice results in embryonic lethality around the peri-implantation stage (14). Recently, YY1 has been shown to play a role in B-cell lineage commitment. B-cell-specific deletion of the *YY1* gene in mice leads to a severe defect in V-to-DJ recombination at the immunoglobulin heavy-chain locus, which blocks the developmental transition from the progenitor B-cell to the precursor B-cell stage (31). In addition, YY1 has been identified as a lineage-specific transcriptional modulator during oligodendrocyte differentiation, regulating the transition from the progenitor to the myelin-forming cell (24).

Multiple studies with animal or tissue culture models have demonstrated an essential role for YY1 in cell proliferation, where YY1 is involved in the transcriptional regulation of a large number of genes essential for cell cycle progression and apoptosis (3, 6, 7, 14). There are also studies linking YY1 to DNA damage response and DNA repair pathways, independent of its transcriptional function. For example, YY1 regulates p53 homeostasis through promoting Hdm2-mediated p53 polyubiquitination (23, 59). Overexpression of YY1 in HeLa cells stimulates PARP-1 enzymatic activity, resulting in accelerated DNA repair (41, 42).

Recently we and others showed that both the drosophila and mammalian YY1 proteins physically interact with the ATP-dependent chromatin remodeling INO80 complex (8, 28, 63) and that together they participate in the maintenance of chromosomal stability and homologous recombination DNA repair in a tissue culture model. However, whether this newly identified role of YY1 in DNA repair has any physiological significance remains unclear. Therefore, we explored YY1 function in mammalian meiosis to address whether YY1 is essential for meiotic homologous recombination DNA repair and to discover other unidentified functions of YY1.

MATERIALS AND METHODS

Generation of the floxed YY1 conditional knockout mice. The generation of the loxP-flanked *yy1* allele (hereinafter called *yy1*^{f}) was described previously (1). Generation of the CD21-Cre3A transgenic mice has been described (29). All

* Corresponding author. Mailing address for Yang Shi: Department of Pathology, Harvard Medical School, New Research Building 854b, 77 Ave. Louis Pasteur, Boston, MA 02115. Phone: (617) 432-4318. Fax: (617) 432-6687. E-mail: yang_shi@hms.harvard.edu. Present address for Su Wu: Whitehead Institute and Department of Biology, Massachusetts Institute of Technology, Cambridge, MA 02142. Phone: (617) 417-0793. Fax: (617) 432-6687. E-mail: swu@wi.mit.edu.

▽ Published ahead of print on 28 September 2009.

mice were bred and maintained under specific-pathogen-free conditions at the animal facility of Harvard Medical School. All mouse protocols were approved by the Harvard Medical School IACUC. Mice are maintained on a mixed background of 129SvEv × C57BL/6.

Histological analysis and TUNEL assay. Animals were killed by cervical dislocation. Testis epididymides and seminal vesicles were examined and weighed. From each male, we fixed one testis and epididymis in Bouin's fixative for 24 h at room temperature and the other testis in phosphate-buffered formalin for 24 h at 4°C. Subsequently, organs were embedded in paraffin. Mounted sections were deparaffinized, rehydrated, and stained with hematoxylin and eosin. For terminal deoxynucleotidyltransferase-mediated dUTP-biotin nick end labeling (TUNEL) analyses, formalin-fixed sections were mounted on glass slides coated with a 2% solution of 3-aminopropyltriethoxysilane in acetone, deparaffinized, and pretreated with proteinase K (Sigma) and peroxidase (20). Slides were subsequently washed in terminal deoxynucleotidyl transferase (TdT) buffer (100 mM cacodylate buffer, 1 mM $CaCl_2$, 0.1 mM dithiothreitol at pH 6.8) for 5 min (22) and incubated for at least 30 min at 25°C in TdT buffer containing 0.01 mM biotin-16-dUTP (Roche Diagnostics) and 0.4 U/μl TdT enzyme (Promega). The enzymatic reaction was stopped in TB buffer (300 mM NaCl, 30 mM Na citrate at pH 7.0), and the sections were washed. Slides were then incubated with StreptAB-Complex-horseradish peroxidase conjugate (Dako) for 30 min and washed in phosphate-buffered saline (PBS). dUTP-biotin-labeled cells were visualized with 3,3′-diaminobenzidine tetrahydrochloride-metal concentrate (Pierce). Next, we counterstained the sections with hematoxylin and counted the number of TUNEL-positive cells per cross-sectioned tubule.

Cytology, IHC, and meiocyte spreading. Paraffin and frozen sections of mouse testis (37), and dry-down (50) or squash (44) preparations of testicular cell suspensions were prepared, incubated for immunocytochemistry, and analyzed as described previously (16, 37). All immunohistochemical (IHC) staining was performed with the serial dilutions of each antibody for the semiquantitative comparison of signal intensities. Antibodies used in this study are as follows. Anti-phospho-histone H2A.X (Ser139) (JBW301), anti-HP1 beta (1MOD-1A9), and anti-HP1 gamma (2MOD-1G6) were purchased from Millipore. Anti-Rad51 (H92) and anti-YY1 (H10 and H414) antibodies were purchased from Santa Cruz Biotechnology. Anti-SCP1 (ab15090), anti-SCP3 (ab15092), anti-H3K27me3 (ab6002), anti-H3K9me2 (ab1220), and anti-H3K9me3 (ab8898) antibodies were purchased from Abcam.

DNA injection and electroporation of testis. Swiss Webster mice purchased from Taconic were used for in vivo DNA electroporation. Male mice at 21 days postpartum were anesthetized with Nembutal solution. Testes were pulled out from the abdominal cavity or scrotum, and approximately 2 μl of plasmid DNA solution was injected into the rete testis using glass capillaries under a binocular microscope as previously described (58). Electric pulses were delivered with an Electrosquare Porator T820 electric pulse generator (BTX). Testes were directly held between a pair of CY650P5 tweezer-type electrodes (Unique Medical Imada, Japan). Square electric pulses were applied twice and again twice in the reverse direction at 30 V for 50 ms for each pulse. The testes were then returned to the abdominal cavity, and the abdominal wall and skin were closed with sutures.

Flow cytometry. The seminiferous tubules of decapsulated testes were dissociated with collagenase, and single-cell suspensions were obtained by trypsin treatment. For immunostaining of SCP1 and SCP3, cells were fixed with 4% paraformaldehyde in PBS, permeabilized with 0.1% Triton X-100 in PBS, and then immunostained with primary antibodies followed by Alexa 546-conjugated goat anti-rat immunoglobulin G or Alexa 546-conjugated goat anti-rabbit immunoglobulin G (Molecular Probes). For cell cycle analysis, cells were fixed with 4% paraformaldehyde in PBS followed by 70% ethanol and stained with 20 μg/ml propidium iodide in PBS containing 400 μg/ml RNase A. The samples were analyzed using a FACSCalibur flow cytometer and the Cell Quest software program (Becton Dickinson). Arithmetic means were used to compare the relative amounts of signals in each gated region.

RESULTS

YY1 localizes to heterochromatin of spermatocytes in mouse testis. The YY1 protein is ubiquitously expressed in the somatic tissues of developing mouse embryos (14), and its nuclear localization has been found in numerous established cell lines, including HeLa, WI38, and human and mouse teratocarcinoma cells (56, 63). High levels of YY1 expression are usually associated with rapid cellular proliferation, consistent with its essential function in cell cycle regulation (1, 14).

While the YY1 role in the soma has been widely studied, little is known about its function in germ cells, the cell type that undergoes meiosis. In this study, we identified a distinct expression pattern of YY1 during spermatogenesis by immmunohistochemistry, with a monoclonal YY1 antibody (H10; Santa Cruz Biotechnology) on testicular sections from juvenile and adult mice (Fig. 1A and B). YY1 is highly expressed in pachytene spermatocytes and at a lower level in zygotene spermatocytes but is not present in leptotene spermatocytes and postmeiotic cells. YY1 is also expressed in spermatogonia at various levels, depending on the stages of seminiferous tubules. A similar immunostaining pattern was observed with a polyclonal YY1 antibody (H414; Santa Cruz Biotechnology) (data not shown). In contrast, these stainings were absent in YY1-deficient spermatogonia and spermatocytes, validating the specificity of the YY1 antibodies we used in this study. Strong YY1 expression appeared in the testes of 3-week-old animals (Fig. 1B-1), a time when the first wave of spermatogenesis reaches the end of meiotic prophase and yields a high percentage of spermatocytes in the testis. At 4 weeks of age (Fig. 1B-2) and in adults (Fig. 1B-3), a high level of YY1 gene expression was still observed in spermatocytes, specifically pachytene cells, but not in round spermatids or spermatozoa (Fig. 1A and B). In addition to germ cells, the supporting cell lineages, i.e., the Sertoli cells and interstitial Leydig cells, were also positive for YY1 staining (Fig. 1A and B).

By immunostaining the meiocyte spreads with a YY1 antibody in combination with SCP3 (Fig. 1C) or gamma-H2AX labeling (Fig. 1D), we found that the YY1 signal was below the level of detection in the leptotene spermatocytes (Fig. 1D-1), low but visible in zygotene spermatocytes, and apparently high on the chromatin of the spermatocytes at the pachytene, diplotene, and diakinesis stages (Fig. 1C and D-2). This is consistent with the immunohistochemical results shown in Fig. 1A and B. Since SCP3 is concentrated at centromeres of spermatocytes during diakinesis and until anaphase I (46), colocalization of YY1 with SCP3 at these stages suggests that YY1 is enriched at centromeres (Fig. 1C-3 and -4). It is also notable that in pachytene spermatocytes, YY1 staining appeared to overlap with the area containing intensive 4′,6′-diamidino-2-phenylindole signals (Fig. 1C-2 to -4 and 1D-2), which preferentially label the AT-rich heterochromatic region, including centromeres (2, 18). Using several reported heterochromatin markers, HP1-beta, H3K9me3 for constitutive heterochromatin (40, 62), and H3K27me3 for facultative heterochromatin (10, 13, 21), we confirmed that YY1 is colocalized with these markers, suggesting that YY1 is concentrated in heterochromatin of spermatocytes (Fig. 1E-1 to -3). We failed to observe colocalization between YY1 and another histone marker, H3K9me2, whose signal was absent in the late pachytene cells (data not shown).

These data suggest stage-dependent expression of YY1 during spermatogenesis. Additionally, its heterochromatin localization in spermatocytes raises the possibility that YY1 may play a role in the regulation of chromatin structure during meiotic prophase.

RNAi knockdown of YY1 in mouse testis causes germ cell aneuploidy and univalent formation. To explore the biological function of YY1 in spermatogenesis, we applied in vivo RNA interference (RNAi) to knock down the expression of the *YY1*

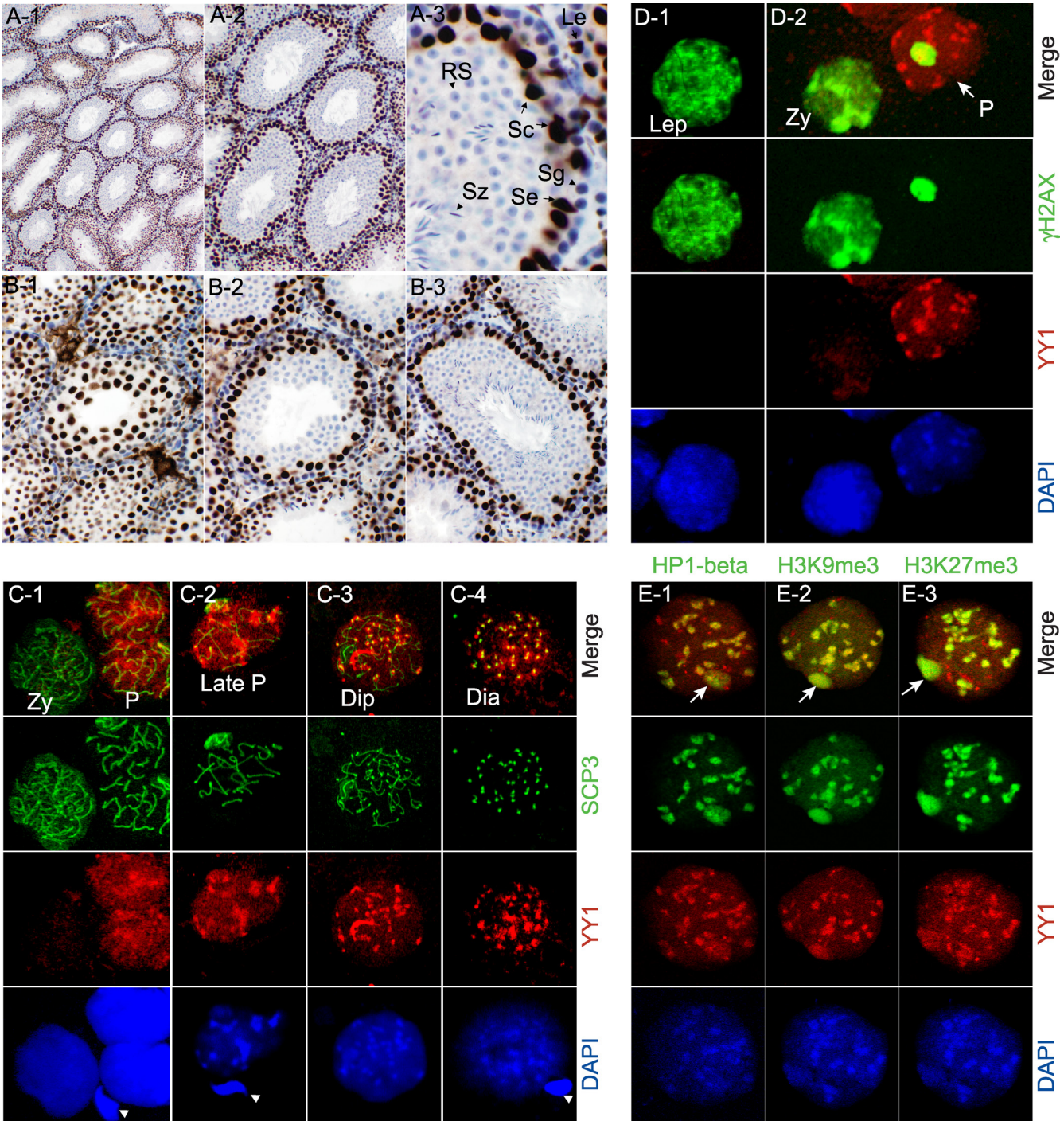

FIG. 1. Immunoanalysis of YY1 expression in mouse testis. (A and B) Histological sections of formalin-fixed, paraffin-embedded testis from a 60-day-old mouse (magnification: A1 and B1, ×100; A2 and B2, ×200; A3 and B3, ×1,000) were stained with YY1 monoclonal antibody (brown). Arrows show YY1 staining in spermatocytes (Sc), spermatogonia (Sg), Sertoli (Se), and Leydig (Le) cells but not in round spermatids (RS) and spermatozoa (Sz) (arrowheads). (C) Meiocyte spreads from mouse spermatocytes were prepared by the drying-down technique and immunolabeled with YY1 (red) and SCP3 (green) antibodies. YY1 appears in zygotene (Zy), pachytene (P), and late pachytene (late P) spermatocytes (C1 and C2) and persists until the diplotene (Dip) and diakinesis (Dia) stages (C3 and C4). Arrowheads indicate elongated spermatids. (D) Meiocyte spreads from the leptotene (Lep), zygotene (Zy), and pachytene (P) spermatocytes were immunostained with both YY1 (red) and gamma-H2AX (green) antibodies. The arrow indicates the pachytene cell. (E) Meiocyte spreads from pachytene spermatocytes were doubly immunostained with YY1 and indicated antibodies. The arrow indicates the sex body.

gene in mouse testis. The in vivo RNAi technique provides a rapid tool for studying gene function in specific tissues and at particular developmental stages (58). To knock down YY1 expression in spermatocytes, we used previously described YY1 short-hairpin RNA (shRNA) constructs (59). Mice at age 21 days postpartum were used because of their high percentage of spermatocytes in the testes. The shRNA plasmid targeting YY1 was coelectroporated with Pgk2-enhanced green fluorescent protein (eGFP) into testes (Fig. 2A and B), where Pgk2 promoter-driven eGFP mainly marks the late spermatocytes and spermatids that take up these plasmids. About 20 to 30% of the total spermatocytes were labeled as GFP positive (Fig. 2C). The spermatogenic cells are connected through intercellular bridges, by which the cytoplasmic materials are shared between spermatocytes. We observed that spermatocytes and spermatids marked by Pgk2-eGFP were clustered (Fig. 2C and D), with similar levels of green fluorescent protein (GFP) expression and YY1 knockdown efficiency within. This suggests that shRNAs can diffuse or be transported through the cytoplasmic bridges (58).

The GFP-positive cells were immunostained with gamma-H2AX in combination with either YY1 or SCP1 antibodies in order to examine the YY1 level and to determine the spermatocyte stages. We confirmed that YY1 was efficiently knocked down by the shRNA, and Pgk2-eGFP was expressed in the expected population (Fig. 2E and F). We then analyzed the DNA content among the GFP-positive cells by flow cytometry 3 days after electroporation (Fig. 2G), when RNAi inhibition of YY1 reached its maximum (data not shown). In the control experiment with a scramble shRNA plasmid, the overall cytometric profile of meiotic and postmeiotic cell populations was similar to what has been reported previously (4). Approximately 41.7% of GFP-labeled cells contained 4N DNA content (primary spermatocytes), and 25.5% had 2N DNA content, indicative of secondary spermatocytes that either are in diakinesis or are binuclear cells before cytokinesis. It has been described previously that the high frequency of 2N population may reflect a high incidence of secondary spermatocytes that complete normal nuclear divisions but fail to undergo cytokinetic cleavage (abortive cytokinesis) (34). In addition, 20.1% of GFP-positive cells contained 1N DNA content, representing spermatids. The 10.1% population with DNA content between 2N and 4N (approximately 3N) may mostly represent aneuploidies resulting from spontaneous meiotic defects (15) (Fig. 2G). In contrast, when YY1 shRNA was introduced, spermatocytes (4N) decreased to approximately 34.0%. Surprisingly, the aneuploidy population with DNA content between 2N and 4N increased by more than twofold in the YY1 knockdown cells (21%) compared with levels in control cells (10.1%), suggesting that YY1 depletion in spermatocytes may impair normal meiotic division. There was an increase of the 2N population in YY1 shRNA-treated testes (30.9%, versus 25.5% for the control), which may have been due to an increase in the secondary spermatocytes remaining in diakinesis or before cytokinesis. These impairments may contribute to the decline of spermatid formation (1N) from 20.1% (scramble shRNA) to 13.4% (YY1 shRNA). A seven-day treatment with YY1 shRNA led to a dramatic reduction of spermatocyte and spermatid populations in testes compared with results for scramble shRNA (Fig. 2H and I). Late spermatocytes from YY1 shRNA-treated testes exhibited cellular degeneration (Fig. 2I2), suggesting a disruption of spermatogenesis during late meiotic prophase.

To further understand how YY1 exerts its regulatory role in meiosis, we isolated GFP-positive spermatocytes and analyzed their SC structures for possible meiotic defects associated with YY1 depletion. Coupled with SCP3 and SCP1 immunostaining (Fig. 2J to M), we observed that a portion of the chromosomes failed to synapse at the chromosomal ends, forming "torch"-like structures in the YY1 knockdown pachytene spermatocytes (Fig. 2L2). In the diplotene stage, SCP1 was retained on the homologous arms in the YY1-depleted spermatocytes (Fig. 2M2), suggesting possible SC disassembly failure. In addition, a fraction of homologous chromosomes appeared to be univalents before anaphase, which may be due to the lack of chiasmata to physically link them together (Fig. 2M2). We noticed that most of the YY1-depleted spermatocytes had more than 20 chromosomes (including paired, unpaired, and broken chromosomes), supporting the finding of univalent formation and aneuploidy. However, the diplotene and metaphase I spermatocytes are rare in the YY1-depleted testes, and this may explain the increased number of abnormal cells with aneuploidy (approximately 3N) in the YY1 knockdown experiments (Fig. 2G). In fact, a similar aneuploidy defect has been found in $YY1^{-/-}$ mouse embryonic fibroblasts (63).

Impaired spermatogenesis and germ cell loss in *YY1*-deleted testes. While using the mice carrying the YY1 conditional allele $YY1^{f/f}$ and the CD21-Cre3A transgene to elucidate the essential role of YY1 during mouse B-cell development (54), we unexpectedly found that the testes from $YY1^{f/f}$/*Cre* (cKO) animals ($n = 5$) were approximately one-third the size of the testes from their $YY1^{f/+}$/*Cre* (Ctr) littermates (Fig. 3A). In contrast, there was no apparent difference in testis sizes and fertility between $YY1^{f/+}$/*Cre* mice and wild-type littermates. We thus investigated the testicular phenotype of the $YY1^{f/f}$/*Cre* mice, in comparison with $YY1^{f/+}$/*Cre* mice as controls. Histological analysis of the testes from cKO mouse revealed abnormal tubule structures (Fig. 3B and C). The tubules of YY1 conditionally null mice contained apparently visible vacuolar structures with fewer pachytene spermatocytes (Fig. 3B2 and C2), while the diameters of individual seminiferous tubules from $YY1^{f/f}$/*Cre* animals were comparable to those of $YY1^{f/+}$/*Cre* littermates.

To confirm YY1 deletion in the $YY1^{f/f}$/*Cre* testes, we performed IHC staining with the YY1 antibody and found that YY1 is specifically deleted in both spermatogonia and spermatocytes in a number of the seminiferous tubules of $YY1^{f/f}$/*Cre* mice (Fig. 3E). A portion of seminiferous tubules in the YY1 conditionally null mice retained YY1 expression in germ cells, which likely resulted from incomplete Cre excision. This type of mosaic deletion by Cre transgenes has been previously found in other testis-specific Cre strains (12). The YY1 expression in Sertoli and Leydig cells was not affected in $YY1^{f/f}$/*Cre* mice, suggesting the activity of CD21-Cre3A is rather germ cell specific (Fig. 3D and 3E). Therefore, the $YY1^{f/f}$/*Cre* mice allowed us to further explore the biological function of YY1 in spermatogenesis and to verify the results from the RNA interference experiments. We were unable to examine the fertility of $YY1^{f/f}$/*Cre* mice due to the premature death at around 3

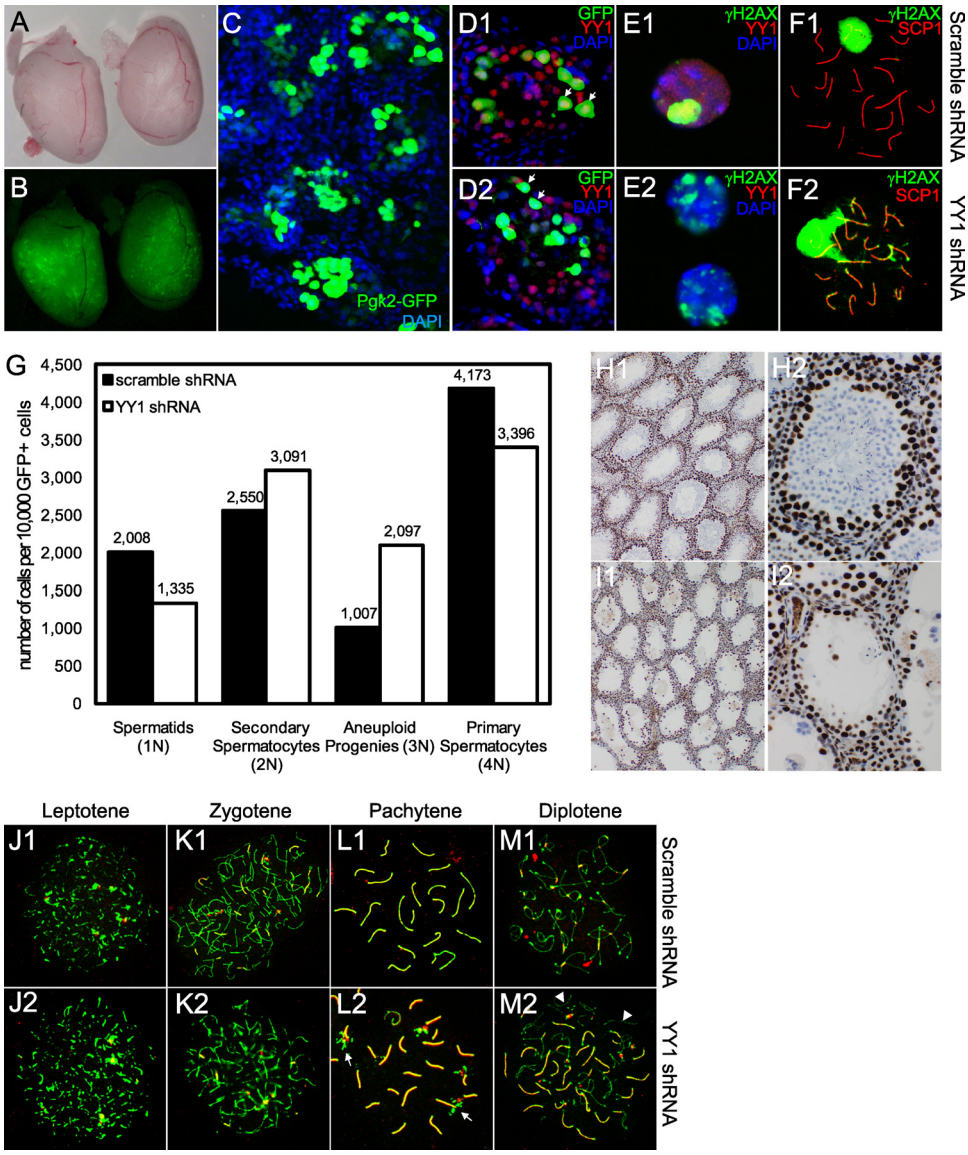

FIG. 2. In vivo RNAi in mouse testis. (A and B) Plasmids expressing YY1 shRNA and scramble shRNA were electroporated into the left and right testes, respectively, of the same animal. Pgk2-eGFP was coelectroporated to label the spermatocytes undertaking the shRNA constructs. (B) Green fluorescence in the mouse testes 3 days after electroporation. YY1 shRNA-treated (left) and scramble shRNA-treated (right) organs are shown. (C) The frozen section of mouse testis shows GFP fluorescence in the spermatocytes eletroporated with Pgk2-eGFP and scramble shRNA plasmids. (D) Immunostaining on the frozen sections of 3-week-old mouse testes treated with scramble shRNA (D1) or YY1 shRNA (D2) for 3 days. The endogenous YY1 level was knocked down with shRNA in spermatocytes compared to the control level (arrows). (E) GFP-positive spermatocytes treated with scramble shRNA (E1) or YY1 shRNA (E2) for 3 days were sorted out by fluorescence-activated cell sorting. Intact spermatocytes were fixed and stained with gamma-H2AX (green) and YY1 (red) antibodies to confirm the cell type and the knockdown efficiency. (F) GFP-positive spermatocytes treated with scramble shRNA (F1) or YY1 shRNA (F2) for 3 days were sorted out by fluorescence-activated cell sorting. Meiocyte spreads were prepared out of sorted cells and stained with gamma-H2AX (green) and SCP1 (red) antibodies. (G) Cell cycle analysis of GFP-positive spermatocytes from shRNA-treated testes. Total cell suspension was prepared out of four mouse testes after a 3-day treatment of shRNA and stained with propidium iodide to monitor the DNA contents. The graph shows the numbers of spermatocytes (4N DNA), aneuploid progenies (approximately 3N DNA), secondary spermatocytes (2N DNA), and spermatids (1N DNA) out of 10,000 GFP-positive cells. (H and I) IHC staining with YY1 antibody (brown) on the seminiferous tubule from scramble shRNA-treated (7 days) mouse testis (magnification: H1, ×100; H2, ×400) and from YY1 shRNA-treated (7 days) mouse testis (magnification: I1, ×100; I2, ×400). (J to M) SCP1 (red) and SCP3 (green) staining on meiocyte spreads from spermatocytes treated with scramble shRNA (J1, K1, L1, and M1) or YY1 shRNA (J2, K2, L2, and M2). Leptotene (J1 and J2), zygotene (K1 and K2), pachytene (L1 and L2), and diplotene (M1 and M2) stages are shown. Arrows indicate "torch"-like structures. Arrowheads indicate univalents.

weeks after birth. Hence, we chose *YY1*$^{f/f}$*/Cre* and *YY1*$^{f/+}$*/Cre* mice at the age of 19 days for further study.

Because an apparent pachytene cell loss is observed in the *YY1*$^{f/f}$*/Cre* testis, we wanted to determine what stages of pachytene cells are missing. We therefore stained the testis sections with the antibody against germ cell nuclear antigen (GCNA), which is known to be highly expressed in the early spermatocytes, such as leptotene, zygotene, and early

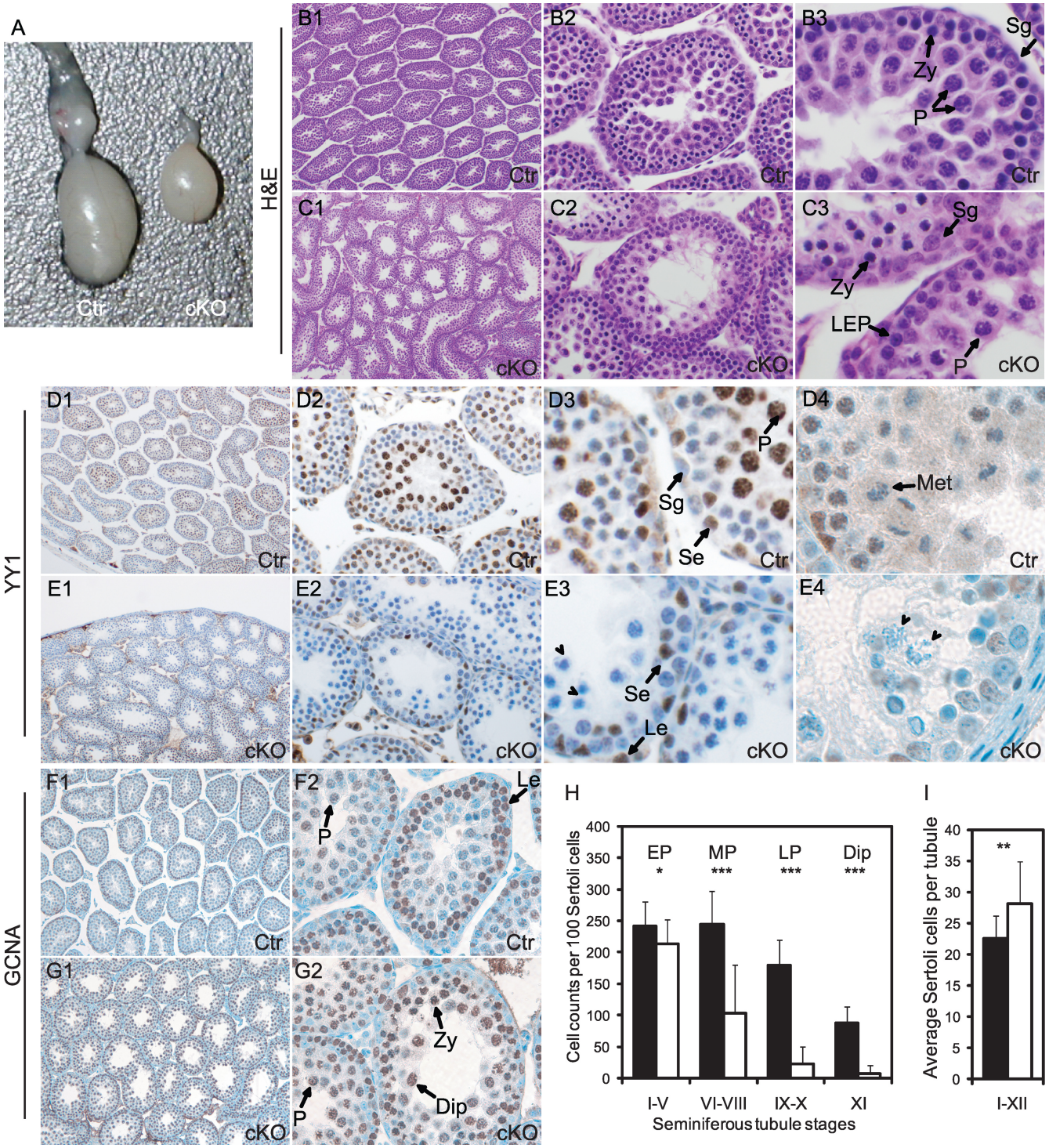

FIG. 3. Defective spermatogenesis in *YY1*$^{f/f}$ *CD21-Cre* mice. (A) Isolated mouse testis from 19-day-old mouse littermates. Ctr, control from *YY1*$^{f/+}$ *CD21-Cre* animal (left); cKO, conditional knockout from *YY1*$^{f/f}$ *CD21-Cre* animal (right). (B and C) Histological sections were stained with hematoxilin and eosin. Testicular histology of 19-day-old control (magnification: B1, ×100; B2, ×400; B3, ×1,000) and conditional knockout (magnification: C1, ×100; C2, ×400; C3, ×1,000) mice is shown. Sg, spermatogonia; LEP, leptotene; Zy, zygotene; P, pachytene. (D and E) IHC staining with YY1 antibody (brown) on the seminiferous tubule from a *YY1*$^{f/+}$ *CD21-Cre* animal (magnification: D1, ×100; D2, ×400; D3, ×600; D4, ×1,000) and from a *YY1*$^{f/f}$ *CD21-Cre* mouse (magnification: E1, ×100; E2, ×400; E3, ×600; E4, ×1,000). Le, Leydig; Se, Sertoli; Sg, spermatogonia; P, pachytene; Met, metaphase I. (F and G) IHC staining with GCNA1 antibody (brown) on the seminiferous tubule from a *YY1*$^{f/+}$ *CD21-Cre* animal (magnification: F1, ×200; F2, ×400) and from a *YY1*$^{f/f}$ *CD21-Cre* mouse (magnification: G1, ×200; G2, ×400). Arrowheads indicate abnormal cells. Le, leptotene; Zy, zygotene; P, pachytene Dip, diplotene. (H) Analysis of cell populations of early (EP), middle (MP), and late (LP) pachytene and diplotene (Dip) spermatocytes from two 19-day-old Ctr and cKO mouse testes. Cells per cross-sectioned seminiferous tubules were counted. To avoid the mosaicism of YY1 deletion in the *YY1*$^{f/f}$/*Cre* testis, the tubules where all the germ cells lack YY1 expression

pachytene cells, but gradually reduced to a much lower level in the mid- and late-pachytene cells (17). We found that the majority of the remaining spermatocytes in the *YY1*$^{f/f}$/*Cre* testis have high levels of GCNA signal, with the patterns indicating that they are leptotene, zygotene, and early pachytene spermatocytes (Fig. 3G1 and 3G2). This result suggests that mid- to late pachytene cells are lost in the *YY1*$^{f/f}$/*Cre* testis. To confirm this observation, we employed a histomorphometric analysis (Fig. 3H) of the testis sections stained with YY1 antibody. To avoid the mosaicism of YY1 deletion in the *YY1*$^{f/f}$/*Cre* testes, we counted only the cells in the tubules where all the germ cells lack YY1 expression. Consistently, we observe a dramatic reduction in the number of pachytene cells along their progression (Fig. 3H), resulting in very few cells reaching the diplotene stage. Interestingly, we found the average number of Sertoli cells per tubule in the *YY1*$^{f/f}$/*Cre* mice to be slightly higher than that in *YY1*$^{f/+}$/*Cre* littermates, perhaps due to the lower cell density of spermatocytes in each tubule (Fig. 3I). In addition, a number of the remaining pachytene cells in the mutant mice had aberrant nuclear morphology (Fig. 3E3 and 3E4). Thus, the loss of YY1 mainly caused a defect in spermatogenesis, especially with the degeneration of pachytene spermatocytes. However, we cannot exclude the remote possibility that systematic defects caused by the infidelity of Cre-mediated YY1 deletion in other organs may contribute to the testis phenotypes. Given the similar spermatogenic phenotypes between the cKO and YY1 RNAi-treated testes, it is likely that the spermatogenic defects seen here are largely due to the loss of YY1 in the germ cells.

Inactivation of YY1 resulting in meiotic DSB accumulation in males. To determine whether the degeneration phenotype of pachytene spermatocytes in *YY1*$^{f/f}$/*Cre* mice was due to cell apoptosis, we carried out the TUNEL assay on testis sections. However, there was no significant increase in the number of cells with typical strong nuclear staining, an indication for apoptotic cells, from YY1 conditionally null testes (Fig. 4A and B) ($P > 0.5$). Surprisingly, we found greatly increased dUTP signals along chromosomes in the *YY1*$^{f/f}$/*Cre* leptotene/zygotene cells compared to those for the control (Fig. 4A and B). It has been shown that the dUTP signal weakly labeled spermatocytes as early as the leptotene stage and up to the zygotene-to-pachytene transition, indicative of meiotic DSBs (35). Thus, this staining on the chromosomes suggests that there are increased chromosome breaks in the *YY1*$^{f/f}$/*Cre* testes, which are probably caused by the unusually high level of meiotic DSBs.

We immunostained the testicular sections from *YY1*$^{f/f}$/*Cre* and *YY1*$^{f/+}$/*Cre* animals with a gamma-H2AX antibody to analyze the meiotic DSB level. In mouse spermatocytes, gamma-H2AX signal is spatially and temporally linked to meiotic DSBs in leptotene/zygotene nuclei and disappears from synapsed autosomes but remains on the sex chromosomes in the pachytene stage (32). The intensity of the gamma-H2AX signal was significantly stronger in *YY1*$^{f/f}$/*Cre* mice than in *YY1*$^{f/+}$/*Cre* mice, especially in the leptotene/zygotene spermatocytes (Fig. 4C and D). This result, together with the observation from the TUNEL assay (Fig. 4A and B), suggests that meiotic DSBs are accumulated in mutant leptotene/zygotene spermatocytes. In the *YY1*$^{f/+}$/*Cre* testes, gamma-H2AX signals disappear from the autosomes after the meiotic DSBs are resolved and are restricted to the sex body in the pachytene stage (Fig. 4C). In *YY1*-deficient pachytene spermatocytes, we observed persistent, albeit low, levels of gamma-H2AX signals on the autosomes, even though the majority of the staining was confined to the sex body (Fig. 4D). Consistent with this phenomenon, we also observed residual gamma-H2AX signals along autosomes in the YY1 shRNA-treated pachytene spermatocyte spreads (Fig. 2E and F). These low-level gamma-H2AX signals are probably caused by chromosomal desynapsis (32) in the *YY1*-deficient spermatocytes, supporting our RNAi results in which chromosome ends fail to synapse in YY1 knockdown pachytene cells (Fig. 2L2). However, we cannot rule out the possibility that it could also be caused by failures to repair those meiotic DSBs in the pachytene cells.

We then addressed the question of whether meiotic recombinations were affected in *YY1*-deficient spermatocytes, using a recombination marker, Rad51. Rad51 is a single-stranded DNA binding protein which is loaded at sites of meiotic DSBs and initiates strand invasion through homologue search (26, 51, 52, 57). Immunolocalization using anti-Rad51 antibody revealed that the protein is detectable as numerous punctuated stainings associated with the developing synapsis during leptotene/zygotene stages (Fig. 4E). In *YY1*-deficient leptotene/zygotene spermatocytes, the level of Rad51 signals was greatly enhanced in comparison with that for the control (Fig. 4E3 and F3), indicating elevated meiotic recombination events. This result, consistent with the findings from the TUNEL assay and gamma-H2AX staining (Fig. 4A to D), suggests accumulation of meiotic DSBs, which lead to increased meiotic recombinations in mutant leptotene/zygotene spermatocytes. These Rad51 staining patterns declined rapidly in the early pachytene cells from the control animals (Fig. 4E2, arrow). In contrast, the Rad51 level remained high in the early pachytene cells of *YY1*-deficient counterparts (Fig. 4F2, arrow), which may be due to chromosomal desynapsis or failure of the resolution of early recombination nodules (39).

Defective heterochromatic state in *YY1*-deficient spermatocytes. It has been shown that heterochromatin is essential to maintain genome stability during male meiosis (49). YY1 is preferentially colocalized with heterochromatin in the spermatocytes, and HP1 was detected in the YY1 protein complex purified from HeLa cells (data not shown). We were interested

were considered for counting. At least 60 tubules were counted for each genotype. EP, MP, LP, and Dip cells were defined by the seminiferous tubule stages I to V, VI to VIII, IX and X, and XI, respectively. The stage XII tubules are rare in both *YY1*$^{f/f}$/*Cre* and *YY1*$^{f/+}$/*Cre* mice at 19 days. Data are represented here as means of the ratio of germ cell number over Sertoli cell number in each tubule ± standard deviation. Black bar, Ctr testes; white bar, cKO testes. (I) Analysis of average Sertoli cell number per tubule among all stages of tubules. Cells per cross-sectioned seminiferous tubule were counted. At least 25 tubules were counted for each genotype. Black bar, Ctr testes; white bar, cKO testes. (*, $P < 0.5$; **, $P < 0.01$; ***, $P < 0.001$).

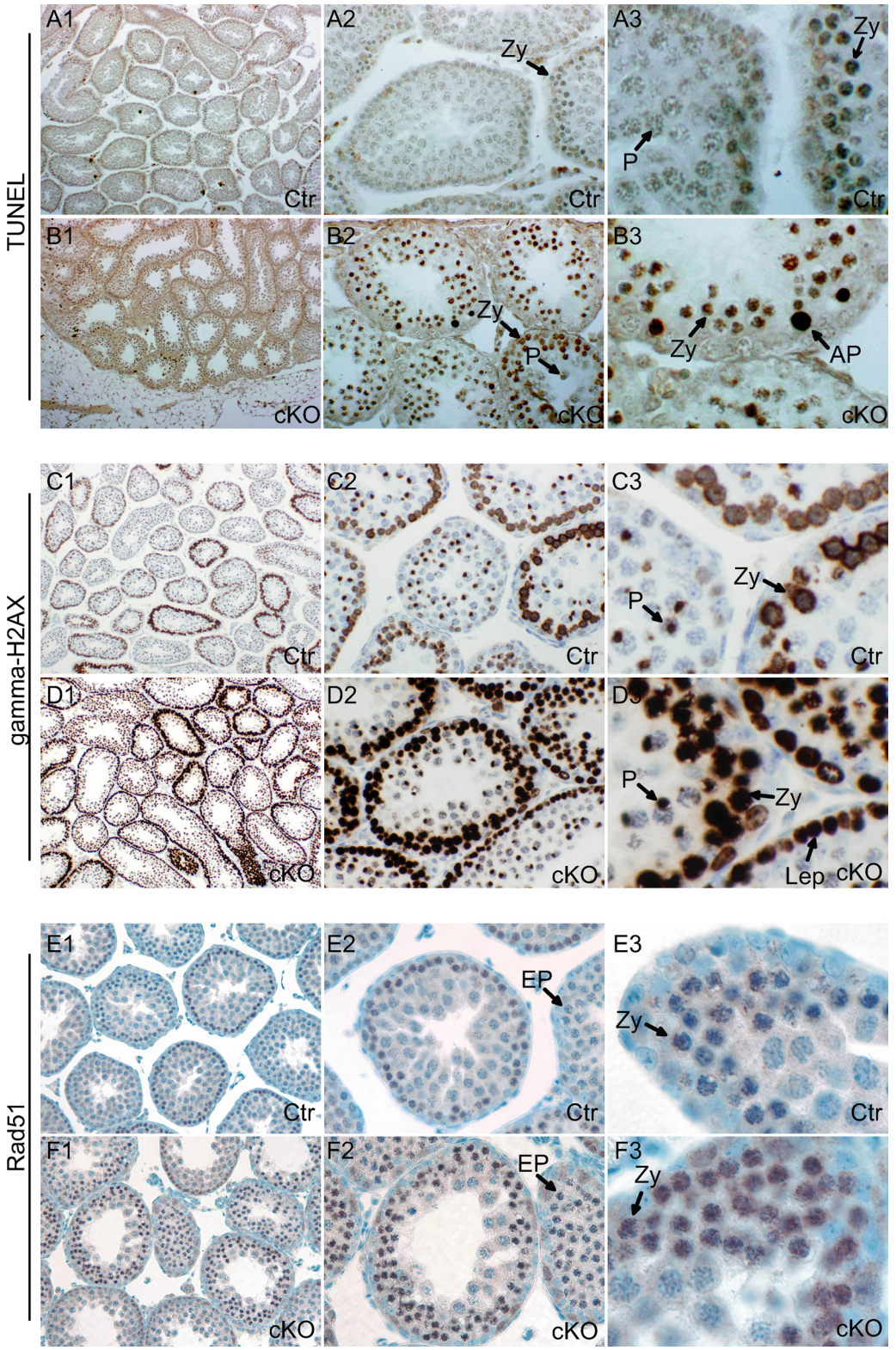

FIG. 4. Meiotic DSB accumulations in *YY1*$^{f/f}$ *CD21-Cre* mice. (A and B) TUNEL analysis on testis sections of *YY1*$^{f/+}$ *CD21-Cre* animal (magnification: A1, ×100; A2, ×400; A3, ×1,000) and *YY1*$^{f/f}$ *CD21-Cre* animal (magnification: B1, ×100; B2, ×400; B3, ×1,000) mice. A few apoptotic nuclei are visible in tubule sections from *YY1*$^{f/f}$ mice. Se, Sertoli; Zy, zygotene; P, pachytene; AP, apoptotic cells. (C and D) IHC staining with gamma-H2AX antibody (brown) on the seminiferous tubule from a *YY1*$^{f/+}$ *CD21-Cre* animal (magnification: C1, ×100; C2, ×400; C3, ×1,000) and from a *YY1*$^{f/f}$ *CD21-Cre* mouse (magnification: D1, ×100X; D2, ×400; D3, ×1,000). Lep, leptotene; Zy, zygotene; P, pachytene. (E and F) IHC staining with Rad51 antibody (brown) in the seminiferous tubule from *YY1*$^{f/+}$ *CD21-Cre* animal (magnification: E1, ×200; E2, ×400; E3, ×1,000) and from a *YY1*$^{f/f}$ *CD21-Cre* mouse (magnification: F1, ×200; F2, ×400; F3, ×1,000). Zy, zygotene; EP, early pachytene.

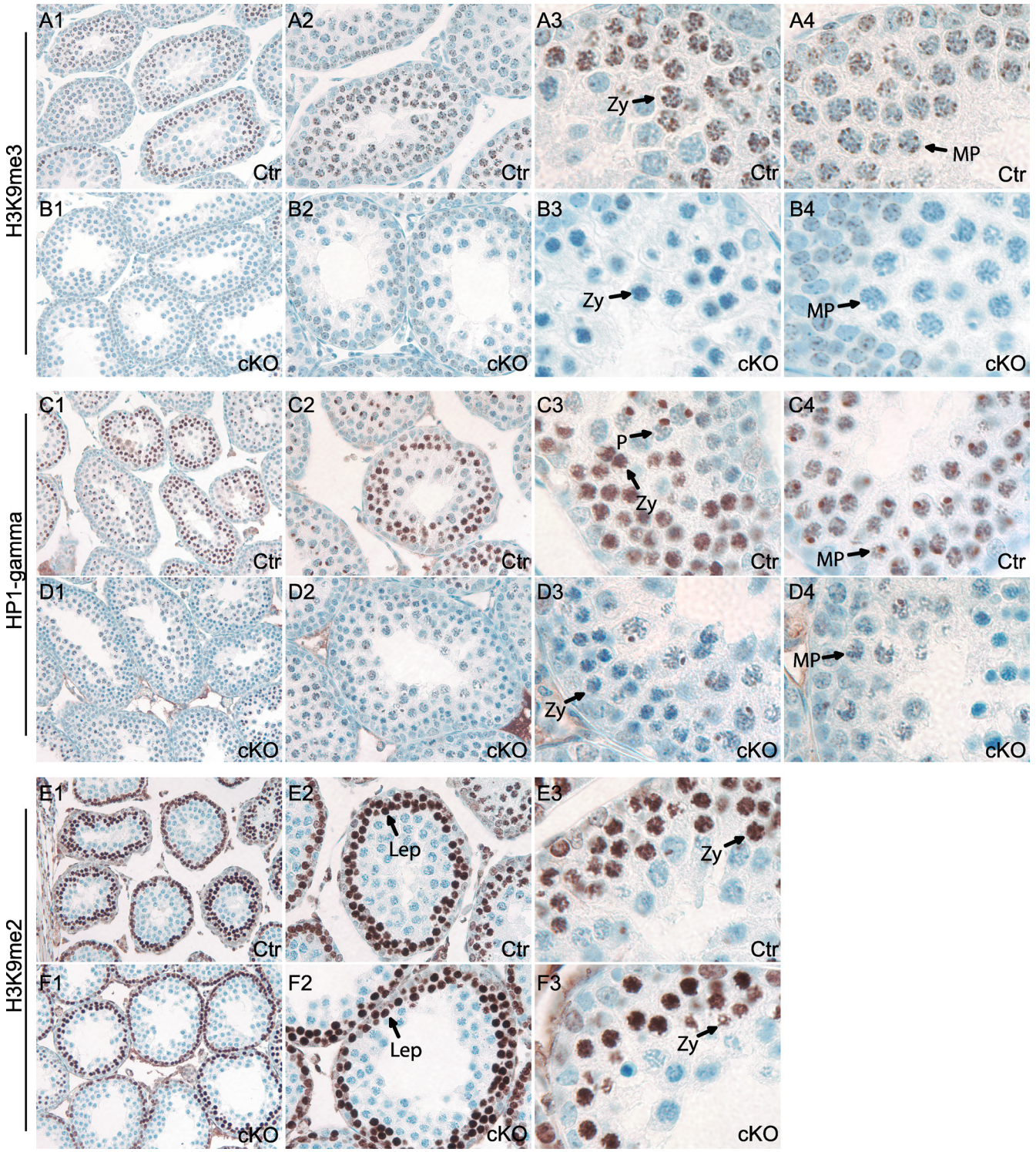

FIG. 5. Defective heterochromatic state in *YY1*$^{f/f}$ *CD21-Cre* mice. (A and B) IHC staining with H3K9me3 antibody (brown) on the seminiferous tubule from a *YY1*$^{f/+}$ *CD21-Cre* animal (magnification: A1, ×200; A2, ×400; A3 and A4, ×1,000) and from a *YY1*$^{f/f}$ *CD21-Cre* mouse (magnification: B1, ×200; B2, ×400; B3 and B4, ×1,000). Zy, zygotene; MP, middle pachytene. (C and D) IHC staining with HP1-gamma antibody (brown) on the seminiferous tubule from a *YY1*$^{f/+}$ *CD21-Cre* animal (magnification: C1, ×200; C2, ×400; C3 and C4, ×1,000) and from a *YY1*$^{f/f}$ *CD21-Cre* mouse (magnification: D1, ×200; D2, ×400; D3 and D4, ×1,000). Zy, zygotene; MP, middle pachytene. (E and F) IHC staining with H3K9me2 antibody (brown) in the seminiferous tubule from *YY1*$^{f/+}$ *CD21-Cre* animal (magnification: E1, ×200; E2, ×400; E3, ×1,000) and from *YY1*$^{f/f}$ *CD21-Cre* mouse (magnification: F1, ×200; F2, ×400; F3, ×1,000). Lep, leptotene; Zy, zygotene.

in determining whether YY1 deletion affected heterochromatin integrity. To examine the heterochromatin status in spermatocytes, we stained the testis sections with an anti-H3K9me3 antibody, a repressive histone marker of heterochromatin (33). In the control section, H3K9me3-labeled heterochromatin was visible in spermatogenic cells, particularly in leptotene/zygotene (Fig. 5A3) and early to-mid pachytene (Fig. 5A4) cells, whereas only residual staining was detected in the *YY1*-deficient testis (Fig. 5B3 and B4).

To confirm this finding, we performed immunostaining on testicular sections with an antibody for HP1-gamma, which is a critical factor for heterochromatin formation and directly interacts with H3K9me3 (11, 33). Similar to H3K9me3 staining, HP1-gamma-labeled heterochromatin was prominent in leptotene/zygotene (Fig. 5C3) and early to mid-pachytene cells (Fig. 5C4), whereas little staining was detected in the *YY1*-deficient testis (Fig. 5D3 and D4). These data suggest that the heterochromatin state may be significantly perturbed in the absence of YY1.

However, in contrast to H3K9me3 and HP1-gamma staining results, we failed to detect much difference between control and cKO testes (Fig. 5E and F) of the level of H3K9me2, a repressive histone marker associated with euchromatin (48). In fact, H3K9me2 nuclear staining was restricted from the leptotene stage until the zygotene stage and absent in pachytene spermatocytes (except for a few sex bodies), suggesting that H3K9me2 has a role different from that of H3K9me3 for meiotic prophase progression (61).

We speculate that the impairment of the heterochromatic state may result in the overproduction of meiotic DSBs and probably defective synapses and chromosome segregations. However, it is unclear at what point of germ cell development YY1 is inactivated by CD21-Cre3A. The phenotypes presented here, including downregulation of heterochromatin markers and accumulation of DSBs, may be a consequence of the loss of YY1 in spermatocytes and/or in cells at the earlier stages, such as spermatogonia and embryonic germ cells.

DISCUSSION

Using genetic and RNAi approaches, we have identified important biological functions of YY1 in mouse spermatogenesis. Depletion of YY1 causes multiple defects in meiotic DSB formation, synapsis, and recombination, which lead to degeneration of spermatocytes. Our study also suggests a role of YY1 in regulating heterochromatin, where we found that deletion of YY1 was correlated with a reduction of the global H3K9me3 and HP1-gamma levels in spermatocytes. Our findings reveal a novel role for YY1 in meiosis during mammalian spermatogenesis.

Chromatin status and meiotic DSB formation. Multiple lines of evidence suggest a link between chromatin status and meiotic DSB formation in various species (5, 53). For instance, HIM-17 is required for proper accumulation of H3K9me2 on germ line chromatin in *C. elegans*. Null mutation of *HIM-17* results in an absence of DSBs, supporting the model that HIM-17 promotes DSB formation through effects on chromosome structure. Other recent examples demonstrating the connections between chromatin states and DSB formation include H3K4me3 (which marks DSB hot spots [5]), H4K16 acetylation (which regulates DSB site distribution [38]), and H3K36 methylation (which regulates DSB hot spot activities [36]). The fact that YY1 seems to be localized on the spermatogenic heterochromatin, which is enriched for H3K9me3 and HP1, and that deletion of YY1 in the germ cells leads to the downregulation of these markers suggests that YY1 is important for regulating heterochromatin in meiotic cells.

Our finding that formation of meiotic DSBs was abnormally increased in YY1 knockout spermatocytes at the leptotene/zygotene stages, in conjunction with decreased levels of H3K9me3 and HP1-gamma (Fig. 5), would also suggest a potential link between these two processes in mammals. Given that heterochromatic regions largely exclude DSB formation as well as gamma-H2AX labeling (27), we propose that the reductions of H3K9me3 and HP1-gamma may alter the structural integrity of heterochromatin, rendering it more accessible to the DSB machinery. However, we cannot rule out the possibility that YY1 might regulate both events independently.

YY1 and meiotic DSB repair. YY1 has been shown to play an essential role in repairing DNA damage through homologous recombination in mammalian cell lines (63). In a reporter assay designed to measure the efficiency of DSB repair by homologous recombination on chromosomes, YY1-deficient cells failed to resolve the introduced DSBs. Consistently, YY1 forms a stable protein complex with INO80, which is known to directly participate in homologous recombination-mediated DNA repair in a number of model organisms (19, 55). Therefore, we speculate that YY1 may also be involved in meiotic DSB repair through homologous recombination. Because a failure of meiotic DNA repair can cause univalent formation at diakinesis (47), the presence of univalents in YY1 knockdown spermatocytes is consistent with this possibility. The univalent formation can lead to the occurrence of aneuploidy in progenies. We observed increased amounts of aneuploidy (approximately 3N in DNA content) in YY1 knockdown spermatocytes, which is consistent with the hypothesis that YY1 takes part in meiotic DSB repair.

In sum, with both in vivo and in vitro approaches, we have demonstrated that YY1 plays a role both in the regulation of chromatin in the spermatogenic cells and in DSB formation during meiosis. Our study suggests a possible link between the modulation of chromatin status and the accumulation of meiotic DSBs in mammals. Our data also suggest that YY1 plays an important role in meiotic DSB repair, which facilitates proper meiotic recombination and homolog segregation. Taken together, our findings identify YY1 as a regulator of mammalian meiosis and therefore provide insights into this important biological process.

ACKNOWLEDGMENTS

We are indebted to Xuecai Ge and Li-Huei Tsai for technical assistance with the in vivo RNAi experiments. We thank Klaus Rajewsky for critical reading of the manuscript and for providing the CD21-Cre3A mice and George C. Enders for the GCNA antibody. We thank the DF/HCC Research Pathology Core and Rodent Histopathology Core for assistance with histology, particularly Roderick Bronson and Jeff Kutok. We thank the Arlene Sharpe laboratory and the optical imaging program of the Harvard NeuroDiscovery Center, particularly Lai Ding, for assistance with microscopy. We thank Monica Colaiacovo for critical reading of the manuscript, the former and current members of the Shi laboratory for unfailing support and encouragement, and the Page laboratory members for scientific discussions.

This work was supported by a grant from the NIH to Y.S. (no. GM053874).

REFERENCES

1. **Affar, E. B., F. Gay, Y. Shi, H. Liu, M. Huarte, S. Wu, T. Collins, E. Li, and Y. Shi.** 2006. Essential dosage-dependent functions of the transcription factor Yin Yang 1 in late embryonic development and cell cycle progression. Mol. Cell. Biol. **26:**3565–3581.
2. **Anderson, L. K., A. Reeves, L. M. Webb, and T. Ashley.** 1999. Distribution of crossing over on mouse synaptonemal complexes using immunofluorescent localization of MLH1 protein. Genetics **151:**1569–1579.
3. **Atchison, L., A. Ghias, F. Wilkinson, N. Bonini, and M. L. Atchison.** 2003. Transcription factor YY1 functions as a PcG protein in vivo. EMBO J. **22:**1347–1358.
4. **Bastos, H., B. Lassalle, A. Chicheportiche, L. Riou, J. Testart, I. Allemand, and P. Fouchet.** 2005. Flow cytometric characterization of viable meiotic and postmeiotic cells by Hoechst 33342 in mouse spermatogenesis. Cytometry A **65:**40–49.
5. **Borde, V., N. Robine, W. Lin, S. Bonfils, V. Geli, and A. Nicolas.** 2009. Histone H3 lysine 4 trimethylation marks meiotic recombination initiation sites. EMBO J. **28:**99–111.
6. **Brown, J. L., C. Fritsch, J. Mueller, and J. A. Kassis.** 2003. The Drosophila pho-like gene encodes a YY1-related DNA binding protein that is redundant with pleiohomeotic in homeotic gene silencing. Development **130:**285–294.
7. **Brown, J. L., D. Mucci, M. Whiteley, M. L. Dirksen, and J. A. Kassis.** 1998. The Drosophila Polycomb group gene pleiohomeotic encodes a DNA binding protein with homology to the transcription factor YY1. Mol. Cell **1:**1057–1064.
8. **Cai, Y., J. Jin, T. Yao, A. J. Gottschalk, S. K. Swanson, S. Wu, Y. Shi, M. P. Washburn, L. Florens, R. C. Conaway, and J. W. Conaway.** 2007. YY1 functions with INO80 to activate transcription. Nat. Struct. Mol. Biol. **14:**872–874.
9. **Cao, L., E. Alani, and N. Kleckner.** 1990. A pathway for generation and processing of double-strand breaks during meiotic recombination in S. cerevisiae. Cell **61:**1089–1101.
10. **Cao, R., L. Wang, H. Wang, L. Xia, H. Erdjument-Bromage, P. Tempst, R. S. Jones, and Y. Zhang.** 2002. Role of histone H3 lysine 27 methylation in Polycomb-group silencing. Science **298:**1039–1043.
11. **Cheutin, T., A. J. McNairn, T. Jenuwein, D. M. Gilbert, P. B. Singh, and T. Misteli.** 2003. Maintenance of stable heterochromatin domains by dynamic HP1 binding. Science **299:**721–725.
12. **Chung, S. S., F. Cuzin, M. Rassoulzadegan, and D. J. Wolgemuth.** 2004. Primary spermatocyte-specific Cre recombinase activity in transgenic mice. Transgenic Res. **13:**289–294.
13. **Czermin, B., R. Melfi, D. McCabe, V. Seitz, A. Imhof, and V. Pirrotta.** 2002. Drosophila enhancer of Zeste/ESC complexes have a histone H3 methyltransferase activity that marks chromosomal Polycomb sites. Cell **111:**185–196.
14. **Donohoe, M. E., X. Zhang, L. McGinnis, J. Biggers, E. Li, and Y. Shi.** 1999. Targeted disruption of mouse Yin Yang 1 transcription factor results in peri-implantation lethality. Mol. Cell. Biol. **19:**7237–7244.
15. **Eichenlaub-Ritter, U.** 1996. Parental age-related aneuploidy in human germ cells and offspring: a story of past and present. Environ. Mol. Mutagen. **28:**211–236.
16. **Eijpe, M., H. Offenberg, R. Jessberger, E. Revenkova, and C. Heyting.** 2003. Meiotic cohesin REC8 marks the axial elements of rat synaptonemal complexes before cohesins SMC1β and SMC3. J. Cell Biol. **160:**657–670.
17. **Enders, G. C., and J. J. May II.** 1994. Developmentally regulated expression of a mouse germ cell nuclear antigen examined from embryonic day 11 to adult in male and female mice. Dev. Biol. **163:**331–340.
18. **Evans, E. P.** 1989. Standard normal chromosomes, p. 576–578. *In* P. M. Lyon and A. G. Searle (ed.), Genetic variants and strains of the laboratory mouse. Oxford University Press, Oxford, United Kingdom.
19. **Fritsch, O., G. Benvenuto, C. Bowler, J. Molinier, and B. Hohn.** 2004. The INO80 protein controls homologous recombination in Arabidopsis thaliana. Mol. Cell **16:**479–485.
20. **Gavrieli, Y., Y. Sherman, and S. A. Ben-Sasson.** 1992. Identification of programmed cell death in situ via specific labeling of nuclear DNA fragmentation. J. Cell Biol. **119:**493–501.
21. **Gilbert, N., S. Boyle, H. Sutherland, J. de Las Heras, J. Allan, T. Jenuwein, and W. A. Bickmore.** 2003. Formation of facultative heterochromatin in the absence of HP1. EMBO J. **22:**5540–5550.
22. **Gorczyca, W., J. Gong, and Z. Darzynkiewicz.** 1993. Detection of DNA strand breaks in individual apoptotic cells by the in situ terminal deoxynucleotidyl transferase and nick translation assays. Cancer Res. **53:**1945–1951.
23. **Gronroos, E., A. A. Terentiev, T. Punga, and J. Ericsson.** 2004. YY1 inhibits the activation of the p53 tumor suppressor in response to genotoxic stress. Proc. Natl. Acad. Sci. USA **101:**12165–12170.
24. **He, Y., J. Dupree, J. Wang, J. Sandoval, J. Li, H. Liu, Y. Shi, K. A. Nave, and P. Casaccia-Bonnefil.** 2007. The transcription factor Yin Yang 1 is essential for oligodendrocyte progenitor differentiation. Neuron **55:**217–230.
25. **Hunter, N., and R. H. Borts.** 1997. Mlh1 is unique among mismatch repair proteins in its ability to promote crossing-over during meiosis. Genes Dev. **11:**1573–1582.
26. **Hunter, N., and N. Kleckner.** 2001. The single-end invasion: an asymmetric intermediate at the double-strand break to double-Holliday junction transition of meiotic recombination. Cell **106:**59–70.
27. **Kim, J. A., M. Kruhlak, F. Dotiwala, A. Nussenzweig, and J. E. Haber.** 2007. Heterochromatin is refractory to gamma-H2AX modification in yeast and mammals. J. Cell Biol. **178:**209–218.
28. **Klymenko, T., B. Papp, W. Fischle, T. Kocher, M. Schelder, C. Fritsch, B. Wild, M. Wilm, and J. Muller.** 2006. A Polycomb group protein complex with sequence-specific DNA-binding and selective methyl-lysine-binding activities. Genes Dev. **20:**1110–1122.
29. **Kraus, M., M. B. Alimzhanov, N. Rajewsky, and K. Rajewsky.** 2004. Survival of resting mature B lymphocytes depends on BCR signaling via the Igα/β heterodimer. Cell **117:**787–800.
30. **Lipkin, S. M., P. B. Moens, V. Wang, M. Lenzi, D. Shanmugarajah, A. Gilgeous, J. Thomas, J. Cheng, J. W. Touchman, E. D. Green, P. Schwartzberg, F. S. Collins, and P. E. Cohen.** 2002. Meiotic arrest and aneuploidy in MLH3-deficient mice. Nat. Genet. **31:**385–390.
31. **Liu, H., M. Schmidt-Supprian, Y. Shi, E. Hobeika, N. Barteneva, H. Jumaa, R. Pelanda, M. Reth, J. Skok, and K. Rajewsky.** 2007. Yin Yang 1 is a critical regulator of B-cell development. Genes Dev. **21:**1179–1189.
32. **Mahadevaiah, S. K., J. M. Turner, F. Baudat, E. P. Rogakou, P. de Boer, J. Blanco-Rodriguez, M. Jasin, S. Keeney, W. M. Bonner, and P. S. Burgoyne.** 2001. Recombinational DNA double-strand breaks in mice precede synapsis. Nat. Genet. **27:**271–276.
33. **Maison, C., and G. Almouzni.** 2004. HP1 and the dynamics of heterochromatin maintenance. Nat. Rev. Mol. Cell Biol. **5:**296–304.
34. **Manandhar, G., R. D. Moreno, C. Simerly, K. Toshimori, and G. Schatten.** 2000. Contractile apparatus of the normal and abortive cytokinetic cells during mouse male meiosis. J. Cell Sci. **113:**4275–4286.
35. **Marcon, L., and G. Boissonneault.** 2004. Transient DNA strand breaks during mouse and human spermiogenesis: new insights in stage specificity and link to chromatin remodeling. Biol. Reprod. **70:**910–918.
36. **Merker, J. D., M. Dominska, P. W. Greenwell, E. Rinella, D. C. Bouck, Y. Shibata, B. D. Strahl, P. Mieczkowski, and T. D. Petes.** 2008. The histone methylase Set2p and the histone deacetylase Rpd3p repress meiotic recombination at the HIS4 meiotic recombination hotspot in Saccharomyces cerevisiae. DNA Repair (Amsterdam) **7:**1298–1308.
37. **Meuwissen, R. L., H. H. Offenberg, A. J. Dietrich, A. Riesewijk, M. van Iersel, and C. Heyting.** 1992. A coiled-coil related protein specific for synapsed regions of meiotic prophase chromosomes. EMBO J. **11:**5091–5100.
38. **Mieczkowski, P. A., M. Dominska, M. J. Buck, J. D. Lieb, and T. D. Petes.** 2007. Loss of a histone deacetylase dramatically alters the genomic distribution of Spo11p-catalyzed DNA breaks in Saccharomyces cerevisiae. Proc. Natl. Acad. Sci. USA **104:**3955–3960.
39. **Moens, P. B., D. J. Chen, Z. Shen, N. Kolas, M. Tarsounas, H. H. Heng, and B. Spyropoulos.** 1997. Rad51 immunocytology in rat and mouse spermatocytes and oocytes. Chromosoma **106:**207–215.
40. **Namekawa, S. H., P. J. Park, L. F. Zhang, J. E. Shima, J. R. McCarrey, M. D. Griswold, and J. T. Lee.** 2006. Postmeiotic sex chromatin in the male germline of mice. Curr. Biol. **16:**660–667.
41. **Oei, S. L., and Y. Shi.** 2001. Poly(ADP-ribosyl)ation of transcription factor Yin Yang 1 under conditions of DNA damage. Biochem. Biophys. Res. Commun. **285:**27–31.
42. **Oei, S. L., and Y. Shi.** 2001. Transcription factor Yin Yang 1 stimulates poly(ADP-ribosyl)ation and DNA repair. Biochem. Biophys. Res. Commun. **284:**450–454.
43. **Orlando, V.** 2003. Polycomb, epigenomes, and control of cell identity. Cell **112:**599–606.
44. **Page, J., J. A. Suja, J. L. Santos, and J. S. Rufas.** 1998. Squash procedure for protein immunolocalization in meiotic cells. Chromosome Res. **6:**639–642.
45. **Page, S. L., and R. S. Hawley.** 2003. Chromosome choreography: the meiotic ballet. Science **301:**785–789.
46. **Parra, M. T., A. Viera, R. Gomez, J. Page, R. Benavente, J. L. Santos, J. S. Rufas, and J. A. Suja.** 2004. Involvement of the cohesin Rad21 and SCP3 in monopolar attachment of sister kinetochores during mouse meiosis I. J. Cell Sci. **117:**1221–1234.
47. **Pasierbek, P., M. Jantsch, M. Melcher, A. Schleiffer, D. Schweizer, and J. Loidl.** 2001. A Caenorhabditis elegans cohesion protein with functions in meiotic chromosome pairing and disjunction. Genes Dev. **15:**1349–1360.
48. **Peters, A. H., S. Kubicek, K. Mechtler, R. J. O'Sullivan, A. A. Derijck, L. Perez-Burgos, A. Kohlmaier, S. Opravil, M. Tachibana, Y. Shinkai, J. H. Martens, and T. Jenuwein.** 2003. Partitioning and plasticity of repressive histone methylation states in mammalian chromatin. Mol. Cell **12:**1577–1589.
49. **Peters, A. H., D. O'Carroll, H. Scherthan, K. Mechtler, S. Sauer, C. Schofer, K. Weipoltshammer, M. Pagani, M. Lachner, A. Kohlmaier, S. Opravil, M. Doyle, M. Sibilia, and T. Jenuwein.** 2001. Loss of the Suv39h histone methyltransferases impairs mammalian heterochromatin and genome stability. Cell **107:**323–337.
50. **Peters, A. H., A. W. Plug, M. J. van Vugt, and P. de Boer.** 1997. A drying-

down technique for the spreading of mammalian meiocytes from the male and female germline. Chromosome Res. **5:**66–68.
51. **Plug, A. W., A. H. Peters, K. S. Keegan, M. F. Hoekstra, P. de Boer, and T. Ashley.** 1998. Changes in protein composition of meiotic nodules during mammalian meiosis. J. Cell Sci. **111:**413–423.
52. **Plug, A. W., J. Xu, G. Reddy, E. I. Golub, and T. Ashley.** 1996. Presynaptic association of Rad51 protein with selected sites in meiotic chromatin. Proc. Natl. Acad. Sci. USA **93:**5920–5924.
53. **Reddy, K. C., and A. M. Villeneuve.** 2004. C. elegans HIM-17 links chromatin modification and competence for initiation of meiotic recombination. Cell **118:**439–452.
54. **Schmidt-Supprian, M., and K. Rajewsky.** 2007. Vagaries of conditional gene targeting. Nat. Immunol. **8:**665–668.
55. **Shen, X., G. Mizuguchi, A. Hamiche, and C. Wu.** 2000. A chromatin remodelling complex involved in transcription and DNA processing. Nature **406:**541–544.
56. **Shi, Y., J. S. Lee, and K. M. Galvin.** 1997. Everything you have ever wanted to know about Yin Yang 1. Biochim. Biophys. Acta **1332:**F49–F66.
57. **Shinohara, A., H. Ogawa, and T. Ogawa.** 1992. Rad51 protein involved in repair and recombination in S. cerevisiae is a RecA-like protein. Cell **69:**457–470.
58. **Shoji, M., S. Chuma, K. Yoshida, T. Morita, and N. Nakatsuji.** 2005. RNA interference during spermatogenesis in mice. Dev. Biol. **282:**524–534.
59. **Sui, G., and Y. Shi.** 2005. Gene silencing by a DNA vector-based RNAi technology. Methods Mol. Biol. **309:**205–218.
60. **Sun, H., D. Treco, N. P. Schultes, and J. W. Szostak.** 1989. Double-strand breaks at an initiation site for meiotic gene conversion. Nature **338:**87–90.
61. **Tachibana, M., M. Nozaki, N. Takeda, and Y. Shinkai.** 2007. Functional dynamics of H3K9 methylation during meiotic prophase progression. EMBO J. **26:**3346–3359.
62. **Takada, Y., K. Isono, J. Shinga, J. M. Turner, H. Kitamura, O. Ohara, G. Watanabe, P. B. Singh, T. Kamijo, T. Jenuwein, P. S. Burgoyne, and H. Koseki.** 2007. Mammalian Polycomb Scmh1 mediates exclusion of Polycomb complexes from the XY body in the pachytene spermatocytes. Development **134:**579–590.
63. **Wu, S., Y. Shi, P. Mulligan, F. Gay, J. Landry, H. Liu, J. Lu, H. H. Qi, W. Wang, J. A. Nickoloff, and C. Wu.** 2007. A YY1-INO80 complex regulates genomic stability through homologous recombination-based repair. Nat. Struct. Mol. Biol. **14:**1165–1172.